Science of the Total Environment 633 (2018) 1032–1040

Contents lists available at ScienceDirect

Science of the Total Environment

journal homepage: www.elsevier.com/locate/scitotenv

Relative contributions of wind and water erosion to total soil loss and its effect on soil properties in sloping croplands of the Chinese Loess Plateau

Dengfeng Tuo [a,b], Mingxiang Xu [a,*], Guangyao Gao [b]

[a] State Key Laboratory of Soil Erosion and Dryland Farming on the Loess Plateau, Institute of Soil and Water Conservation, Northwest A&F University, Yangling, Shaanxi 712100, China
[b] State Key Laboratory of Urban and Regional Ecology, Research Center for Eco-Environmental Sciences, Chinese Academy of Sciences, Beijing 100085, China

HIGHLIGHTS

- This study quantified the contributions of wind and water erosion to total erosion.
- The sites with most serious erosion and nutrient loss located in the upper positions on northwest-facing slopes.
- Complex erosion by wind and water accelerated the degradation of the soil quality.
- Control water erosion could more effectively reduce soil loss compared to the control wind erosion.

GRAPHICAL ABSTRACT

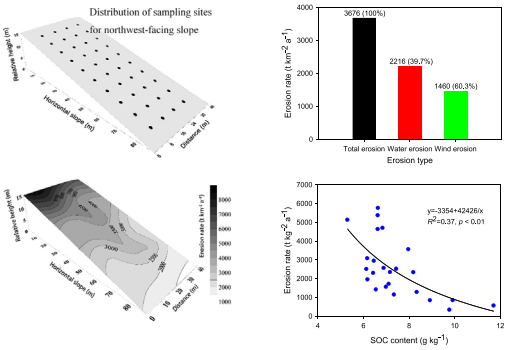

ARTICLE INFO

Article history:
Received 14 January 2018
Received in revised form 20 March 2018
Accepted 20 March 2018
Available online 28 March 2018

Editor: Jay Gan

Keywords:
^{137}Cs
RUSLE model
Erosion rate
Soil organic carbon
Slope aspect

ABSTRACT

Wind and water erosion are two dominant types of erosion that lead to soil and nutrient losses. Wind and water erosion may occur simultaneously to varying extents in semi-arid regions. The contributions of wind and water erosion to total erosion and their effects on soil quality, however, remains elusive. We used cesium-137 (^{137}Cs) inventories to estimate the total soil erosion and used the Revised Universal Soil Loss Equation (RUSLE) to quantify water erosion in sloping croplands. Wind erosion was estimated from the subtraction of the two. We also used ^{137}Cs inventories to calculate total soil erosion and validate the relationships of the soil quality and erosion at different slope aspects and positions. The results showed that wind erosion (1460 t km^{-2} a^{-1}) on northwest-facing slope was responsible for approximately 39.7% of the total soil loss, and water erosion (2216 t km^{-2} a^{-1}) accounted for approximately 60.3%. The erosion rates were 58.8% higher on northwest- than on southeast-facing slopes. Northwest-facing slopes had lower soil organic carbon, total nitrogen, clay, and silt contents than southeast-facing slopes, and thus, the ^{137}Cs inventories were lower, and the total soil erosions were higher on the northwest-facing slopes. The variations in soil physicochemical properties were related to total soil erosion. The lowest ^{137}Cs inventories and nutrient contents were recorded at the upper positions on the northwest-facing slopes due to the successive occurrence of more severe wind and water erosion at the same site. The results indicated that wind and water could accelerate the spatial variability of erosion rate and soil properties and cause serious decreases in the nutrient contents in sloping fields. Our research could help researchers develop soil strategies to reduce soil erosion according to the dominant erosion type when it occurs in a hilly agricultural area.

* Corresponding author.
E-mail address: xumx@nwsuaf.edu.cn (M. Xu).

https://doi.org/10.1016/j.scitotenv.2018.03.237
0048-9697/

1. Introduction

Erosion by the forces of either wind or water is an important cause of soil degradation and reduction in plant productivity in agricultural areas (Galy et al., 2015; Du et al., 2017; Van Pelt et al., 2017). Although water and wind erosion are two common types of erosion and may occur in specific climatic zones: wind erosion in drier regions, and water erosion in wetter regions, erosion is complex in semi-arid environments, as combinations of wind and water erosion occurs on both temporal and spatial scales (Visser and Sterk, 2007; Tuo et al., 2016).

Many researchers have analyzed the importance of wind and water erosion processes (Song et al., 2005; Tuo et al., 2016; Wang et al., 2016). Wind-driven sediment can be deposited directly into channels, where it is stored until fluvial process to transport the sediment down the channel (Belnap et al., 2011). According to long-term monitoring in terraces, Van Pelt et al. (2017) showed that wind erosion is a larger component of net soil redistribution than water erosion. In an experiment that was first conducted with wind erosion and then with water erosion, Tuo et al. (2016) noted that wind erosion clearly has the capacity to intensify water erosion. In addition, some studies reported that the erosion change depended on natural factors and human factors (Du et al., 2017; Xue et al., 2017). Martínez-Graña et al. (2014, 2015) used a cartographic method to show a high risk of water erosion in areas with high slopes and elevations and little agricultural activity. The risk of wind erosion is higher in sectors with low vegetation cover and highly erodible textures. Although these studies could help soil conservation researchers develop strategies to reduce total soil loss, quantitative analysis of wind and water erosion is a complex task (Zhang et al., 2011; Wang et al., 2016), and few studies have been conducted to distinguish a single erosion from the total erosion and its relationship to soil quality (Breshears et al., 2003; Song et al., 2005; Zhang et al., 2018). These problems hinder the recognition of the consequences of erosion in regions where both types of erosion occur (Visser et al., 2004).

The greatest obstacle in partitioning wind and water erosion is the limitation of feasible methods and techniques to measure wind erosion compared to water erosion (Van Pelt et al., 2017). Previous studies for quantifying wind and water erosion by sampling and monitoring required many years and many points in a field (Zhang et al., 2011). Experiments that combined wind tunnels with simulated rainfall supported integrated research. Tuo et al. (2015, 2016) studied wind and water erosion to investigate the characteristics of runoff, sediment, and soil particles under a one-way wind erosion-rain erosion sequence. Breshears et al. (2003) compared the horizontal mass transport of wind- and water-driven materials in different semi-arid ecosystems. However, these techniques basically examined bare soil at horizontal wind velocity, the other conditions remain unknown. The measurements of sediment by wind and water are not necessarily indicative of relative soil erosion rates (Zhang et al., 2011). Recent studies suggested that model simulations for estimating soil redistribution across a landscape could produce a plausible result and provide a better understanding of wind and water erosion processes (Schmidt et al., 2017; Zhang et al., 2018).

Cesium-137 (^{137}Cs) has been widely applied as a surrogate to total soil erosion studies on almost every continent (Van Pelt et al., 2017) and has been used to determine the impacts of soil erosion on nutrient dynamics in a wide range of agricultural landscapes (Afshar et al., 2010; Nie et al., 2013). ^{137}Cs is an artificial radionuclide (half-life of 30.17 years) that was released into the environment as a result of nuclear weapons tests primarily during the 1950s–1970s (Fang et al., 2012). The use of ^{137}Cs to estimates of soil redistribution relies on four hypotheses (Parsons and Foster, 2011). First, ^{137}Cs fallout is spatially and locally uniform. Second, the fallout is rapidly fixed onto soil particles. Third, the subsequent ^{137}Cs redistribution is due to the movement of soil particles. Fourth, there is a reference site that should be undisturbed and representative of the entire study area. Finally, the estimates of soil erosion can be derived from measurements of ^{137}Cs inventories.

The Revised Universal Soil Loss Equation (RUSLE) models soil loss to water erosion as a function of climate erosivity (the degree to which rainfall can result in erosion), topography, soil erodibility, and land management (Bowker et al., 2008). The RUSLE model is the most widely used empirical model to calculate water erosion at both basin and field scales resulting from sheet and rill erosion (Conforti et al., 2016; Conforti and Buttafuoco, 2017). Unlike process-based models such as WEPP and EUROSEM, the RUSLE model usually does not require extensive input data and calibration efforts (Tiwari et al., 2000; Khaleghpanah et al., 2016). The RUSLE model has its advantages over the process-based models, because it is accurate and easy to use in terms of parameterization (Gao et al., 2012). Li et al. (2017a) even noted that RUSLE models could produce sound predictions in the Chinese Loess Plateau.

This study selected typical sloped croplands with different aspects and positions on a field scale in the wind-water erosion crisscross region of the Chinese Loess Plateau. All sites were higher than the surrounding landforms and vegetation, and thus, soils at the surface were subject to erosion by water and wind. ^{137}Cs was used to estimate the total soil erosion, and the RUSLE model was used to quantify water erosion. Wind erosion results from the subtraction of water erosion from total soil erosion. In addition, we used ^{137}Cs to calculate the total soil erosion and soil physicochemical properties on slopes with different aspects and positions. The objectives of this study were to (1) quantify the contributions of wind and water erosion to total erosion in sloping croplands, and (2) investigate the relationships between total soil erosion and physicochemical properties for different slope conditions.

2. Materials and methods

2.1. Study area

The study area was located in the wind-water erosion crisscross region on the Chinese Loess Plateau (37°13′N, 107°56′E; Fig. 1). The average elevation of the area ranged from 1577 to 1705 m AMSL. The area is characterized by a semiarid climate, with a mean annual temperature of 7.9 °C and a mean annual precipitation of 361.9 mm. The rainfall was typically high-intensity and short duration rainstorms. The soils are classified as typical loessial soil, which originated from wind deposits and are characterized by the absence of bedding, a silty texture, looseness, and macroporosity, with an average thickness of 50–80 m on the Loess Plateau (Gao et al., 2017). Cropland is the main land use in the region because most of the native vegetation has been cleared due to the long history of crop production, resulting in severe soil erosion, land degradation and soil fertility loss (Jia et al., 2017). The crops in this area were mainly millet (*Setaria italica*), potato (*Solanum tuberosum*), and maize (*Zea mays* L.).

The soil in the study area is subjected to both wind and water erosion. Wind erosion is dominant during the winter and spring, and water erosion is dominant during rainy summers and the autumn. The main wind direction is from the northwest, followed by north and west. Wind rarely comes from the southeast. According to the China Meteorological Data Network, the annual northwest, north, and west winds in the study area (Dingbian County, China) accounted for 91.6, 4.8, and 3.6%, respectively, of the total wind in 2012–2014. The annual average wind speed is 3.2 m s^{-1}. The annual average days of wind speed >6 m s^{-1} are 32, and these mainly occur in March, April, May, November, and December. By contrast, the monthly average precipitation is >60 mm in July, August, and September.

2.2. Selection of study sites and soil sampling

In the April of 2014, we selected land on northwest-facing slope (defined as S7, Table 1) with a long slope length (approximately 105 m) and a uniform slope gradient (approximately 10°) to investigate the

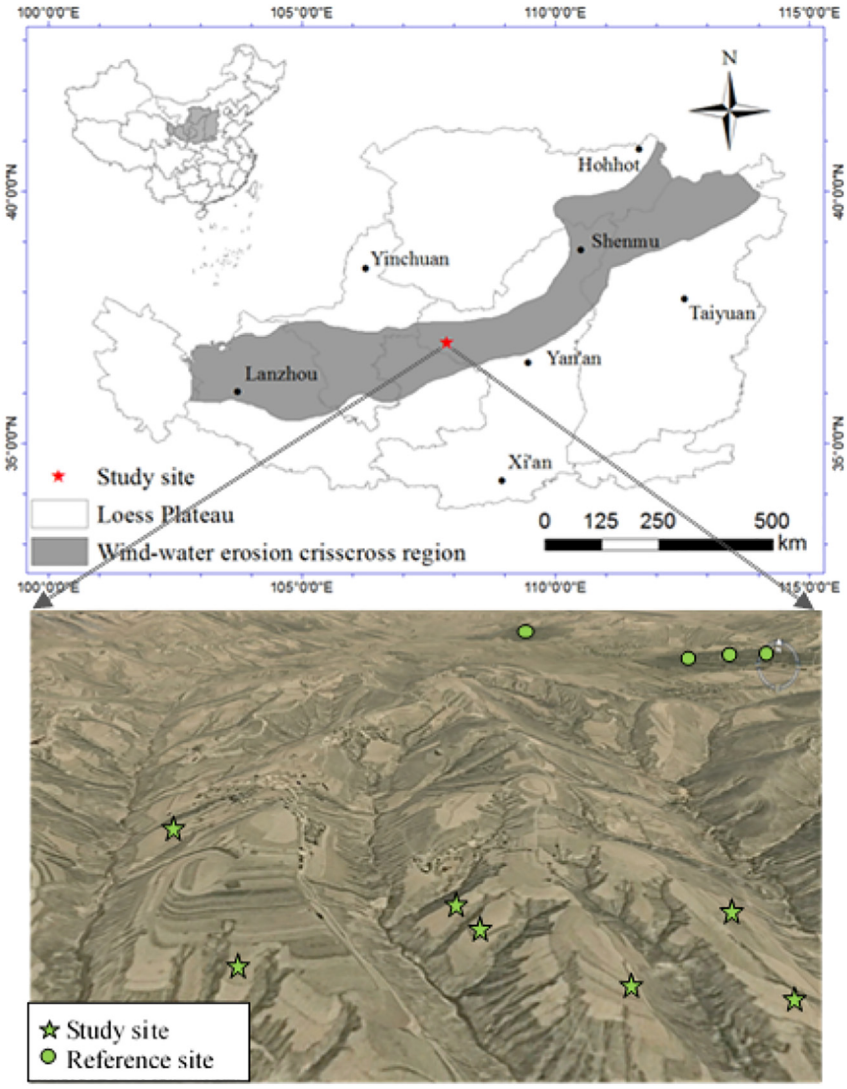

Fig. 1. The locations of the study site and reference site.

water erosion and total soil loss using the RUSLE model and ^{137}Cs measurements. The slope (*Setaria italica*) was higher than the surrounding landforms and the vegetation and soils directly at the surface were subject to erosion by water and wind. For the entire slope, 40 sampling points were collected from the surface soil (20 cm) using a 5-cm-diameter hand-operated core sampler for the determination of soil ^{137}Cs inventories. Soil bulk density (BD) of the 0–20 cm layer was measured at each adjacent sampling point using a soil bulk sampler with a 5-cm diameter and 5-cm-high stainless-steel cutting ring. All sampling points were equally spaced and evenly distributed on the sloped land.

Table 1
Detailed information for the study sites.

	Site	Slope aspect	Average slope gradient (°)	Slope length (m)	Average altitude (m)
Northwest-facing slopes	S1	NW20°	17	80	1647
	S2	NW10°	16	95	1602
	S3	NW32°	22	75	1637
Southeast-facing slopes	S4	SE15°	18	80	1617
	S5	SE30°	17	85	1678
	S6	SE17°	21	75	1607
Northwest-facing slopes	S7	NW15°	10	105	1640

In addition, six cropland sites were selected (three on northwest-facing slopes and three on southeast-facing slopes, defined as S1–S3 and S4–S6, respectively; Table 1) based on exploratory visits and interviews with local farmers. These sites were adjacent to each other and had similar previous farming practices. Millet (*Setaria italica*) was the main crop grown on these six slopes. The slopes were ploughed, smoothed, left bare after harvest, and had never been irrigated. The slope gradients ranged from 16 to 22°, the slope lengths ranged from 75 to 95 m, and the elevations ranged from 1602 to 1678 m. For each slope, four sample positions were established at equal intervals, including upper, middle, lower, and bottom. Each position included three points along a horizontal transect. A 5-cm-diameter hand operated core sampler was used to collect soil samples to a depth of 20 cm for measuring the soil ^{137}Cs inventories. In addition, soil samples were collected from 0 to 5, 5–10, and 10–20 cm layers using a soil drilling sampler (4 cm inner diameter). Soil samples were collected from three points and then mixed to form one soil sample in each soil layer for measuring the physico-chemical properties.

Four reference ^{137}Cs inventories of the soil samples were collected to a depth of 20 cm using a 5 cm diameter soil auger from a nearby site (within 1 km) in an uncultivated, mature, naturally restored *Locust* forest. These sites had not been affected by soil erosion or deposition over the last 55 years.

2.3. Soil sample analysis

The soil samples were air-dried, weighed, crushed, and passed through a 2-mm mesh screen. A 400-g sample was used to measure the ^{137}Cs activity using a hyperpure coaxial germanium detector linked to a multichannel digital analyser. ^{137}Cs inventories were detected at the 662 keV peak over a counting time of 80,000 s, which provided an analytical precision of ±5% for ^{137}Cs at the 95% confidence level (An et al., 2014).

The soil organic carbon (SOC) content was determined by the potassium dichromate volumetric method (Nelson and Sommer, 1982). The total nitrogen (TN) content was measured by the semi-micro Kjeldahl method (Bremner and Mulvaney, 1982). The BD was calculated depending on the volume of the core sampler and the oven-dried weight of the undisturbed soil samples. Soil particle-size distribution was analyzed by laser diffraction (Mastersizer 2000, Malvern Instruments, Malvern, England).

2.4. Partitioning the contributions of wind and water to soil erosion

In the study, the ^{137}Cs inventory was used to estimate the total soil erosion for the northwest-facing slope (S7) on the hilly landscape, and the RUSLE model was used to calculate water erosion. The wind erosion was the result of the subtraction of the two methods.

Mass balance models have frequently been used to establish calibration relationships, which consider the removal of freshly deposited ^{137}Cs fallout (by erosion) before its incorporation into the ploughed layer in cultivated soils. In this model, sampling sites that had lower ^{137}Cs inventories than the reference site inventory were regarded as eroding sites; in contrast, sampling sites that had higher ^{137}Cs inventories than the reference site inventory were regarded as depositional sites. In our study, the ^{137}Cs inventories of all sampling sites were less than the reference site inventory.

For an eroding point, erosion rate can be calculated from the following equation (Walling and He, 1999):

$$\frac{dA(t)}{dt} = (1-\Gamma)I(t) - \left(\lambda + P\frac{R}{d}\right)A(t) \quad (1)$$

where R the erosion rate (kg m^{-2} a^{-1}), $A(t)$ is the cumulative ^{137}Cs activity per unit area (Bq m^{-2}), d the cumulative mass depth representing the average plough depth (kg m^{-2}), λ the decay constant for ^{137}Cs (a^{-1}), $I(t)$ is the annual ^{137}Cs deposition flux (Bq m^{-2} a^{-1}); Γ is the percentage of the freshly deposited ^{137}Cs fallout removed by erosion before being mixed into the plough layer, and P is the particle size correction factor.

The modified RUSLE model predicts long-term average annual water erosion using six factors that are associated with climate, soil, topography, vegetation and management and is calculated as follows (Rendard et al., 1997):

$$A = R \times K \times LS \times C \times P \quad (2)$$

where A is the average water erosion rate (t km^{-2} a^{-1}), R is the rainfall erosivity factor (MJ mm ha^{-1} h^{-1}), K is the soil erodibility factor (t h MJ^{-1} mm^{-1}), LS is the slope-length and steepness factor, C is the cover management factor, and P is the conservation support practice factor.

In this study, the R value is defined as 1345 MJ mm/(ha h), which was taken from the result obtained by Qin et al. (2009) in this study area. EPIC was used to model the K value for bare soil as (Sharply and Williams, 1990):

$$K = \left\{0.2 + 0.3\ exp\left[-0.0256S_a\left(1-\frac{S_i}{100}\right)\right]\right\}\left(\frac{S_i}{C_l + S_i}\right)^{0.3} \times \left[1-\frac{0.25SOC}{SOC + exp(3.72-2.95SOC)}\right]\left[1-\frac{0.7S_n}{S_n + exp(-0.51+22.9S_n)}\right] \quad (3)$$

where S_a is the sand content (%), S_i is the silt content (%), C_l is the clay content (%), SOC is the soil organic carbon content (%), and $S_n = 1 - S_a/100$. The LS factor is calculated according to the following relationships (Nearing, 1997; Qin et al., 2009):

$$L = \left(\frac{l}{22.13}\right)^m \quad (4)$$

$$m = \begin{cases} 0.2, & \theta \le 0.5^\circ \\ 0.3, & 0.5^\circ < \theta \le 1.5^\circ \\ 0.4, & 1.5^\circ < \theta \le 2.5^\circ \\ 0.5, & \theta > 2.5^\circ \end{cases} \quad (5)$$

$$S = -1.5 + \frac{17}{1 + exp(2.3-6.1\ sin\theta)} \quad (6)$$

where l is the slope length (m), m is a variable slope-length exponent, and θ is the slope angle (°). As there is no soil conservation practice for the plot, the P and C factors are set to be 1 ($P = 1$, $C = 1$).

2.5. Statistical analysis

The data are expressed as the means ± standard deviations. One-way ANOVAs were used to determine the significance of the differences in the soil properties among the slope positions and soil depths. Significance was evaluated at the 0.05 level ($p < 0.05$). When significance was observed at the $p < 0.05$ level, a least significant difference (LSD) test was used to conduct multiple comparisons. Pearson correlation coefficients between the ^{137}Cs inventories and soil properties were calculated to analyse the significance of the correlations. Regression analyses were used to determine the relationships between the ^{137}Cs inventories and SOC and TN contents. All of the above statistical tests were conducted using SPSS version 18.0 (SPSS Inc., Chicago, IL, USA). Spatial distributions of soil ^{137}Cs inventories and erosion rates were obtained through the Kriging method using the software surfer 8.0 (Golden Software Inc.).

3. Results

3.1. Erosion rates by wind and water based on ^{137}Cs measurements and the RUSLE model

The descriptive statistic results of ^{137}Cs inventories for the slope site (S7) and reference site are shown in Table 2. For the reference site, the measured inventories were 1449 Bq m^{-2}, with a maximum value of 1521 Bq m^{-2}, a minimum value of 1376 Bq m^{-2}, and a coefficient of variation 4%. For the slope site, the ^{137}Cs inventories ranged

Table 2
Descriptive statistical analysis of ^{137}Cs inventories, erosion thickness and rate on sloping land (S7) and reference site.

	Variables	Minimum	Maximum	Mean	Median	Variation coefficient (%)
Reference site	^{137}Cs inventory (Bq m^{-2})	1376	1521	1449	1449	4
Sloping land	^{137}Cs inventory (Bq m^{-2})	240	1049	690	194	28
	Erosion thickness (cm a^{-1})	0.13	0.69	0.31	0.13	41
	Erosion rate (t km^{-2} a^{-1})	1513	8314	3731	1539	41

from 240 to 1049 Bq m^{-2}, with an average of 690 Bq m^{-2} and a coefficient of variation of 28%. In addition, there were large differences between the minimum and maximum values of the erosion thickness and erosion rate for the entire slope (Table 2). The erosion rates ranged from 1513 to 8314 t km^{-2} a^{-1}, with an average value of 3731 t km^{-2} a^{-1} and a coefficient of variation of 41%. Moreover, the variations in the ^{137}Cs inventories and erosion rates were affected by the slope position. The ^{137}Cs inventories in the upper part of the slope were lower than those in the bottom part of the slope, and an increasing trend from top to bottom occurred along the slope (Fig. 2a). The erosion rate showed a decreasing trend from the top to the bottom of the slope, which is opposite of the ^{137}Cs inventory trend (Fig. 2b).

In this study, the ^{137}Cs inventory was used to estimate the degree of total soil erosion, and the RUSLE was used to quantify water erosion. The wind erosion is the result of the subtraction of the two. The results of the ^{137}Cs measurements showed that the total soil erosion was 3676 t km^{-2} a^{-1}, and the results of the RUSLE model showed that the water erosion was 2216 t km^{-2} a^{-1}. Thus, wind erosion was responsible for approximately 37.9% of the total soil erosion.

3.2. Differences in erosion rates in various slope aspects and positions

The variations in the ^{137}Cs inventories and erosion rates among the slope aspects (SAs) and slope positions (SPs) were obtained for the S1-S6 sites (Fig. 3). The ^{137}Cs inventories ranged from 828 to 1129 Bq m^{-2} and 526 to 908 Bq m^{-2} on the southeast- and northwest-facing slopes, respectively (Fig. 3a). The average ^{137}Cs inventory was 26.8% higher on the southeast- than northwest-facing slopes. In addition, the inventories increased from the tops to the bottoms of the slopes. The ^{137}Cs inventories were lower on the upper SPs than on the bottom SPs for both SAs (Fig. 3a). The spatial patterns of the erosion rates on the SAs and SPs were similar to those of the ^{137}Cs inventories. The erosion rate varied from 2516 to 4814 t km^{-2} y^{-1} on the northwest-facing slopes, with a mean of 3396 t km^{-2} y^{-1}, and from 1525 to 2750 t km^{-2} y^{-1} on the southeast-facing slopes, with a mean of 2139 t km^{-2} y^{-1} (Fig. 3b). The average erosion rate in the study area was 2768 t km^{-2} y^{-1}. The site with the most serious erosion (approximately 4814 t km^{-2} y^{-1}) was at the top of a northwest-facing slope.

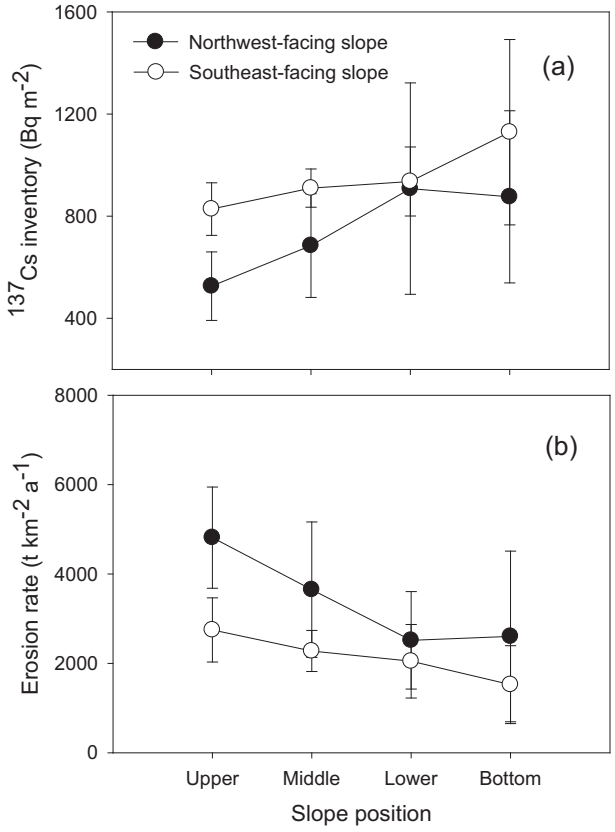

Fig. 3. Soil ^{137}Cs inventories (a) and erosion rates (b) for the slope aspects and positions (slope sites S1–S6).

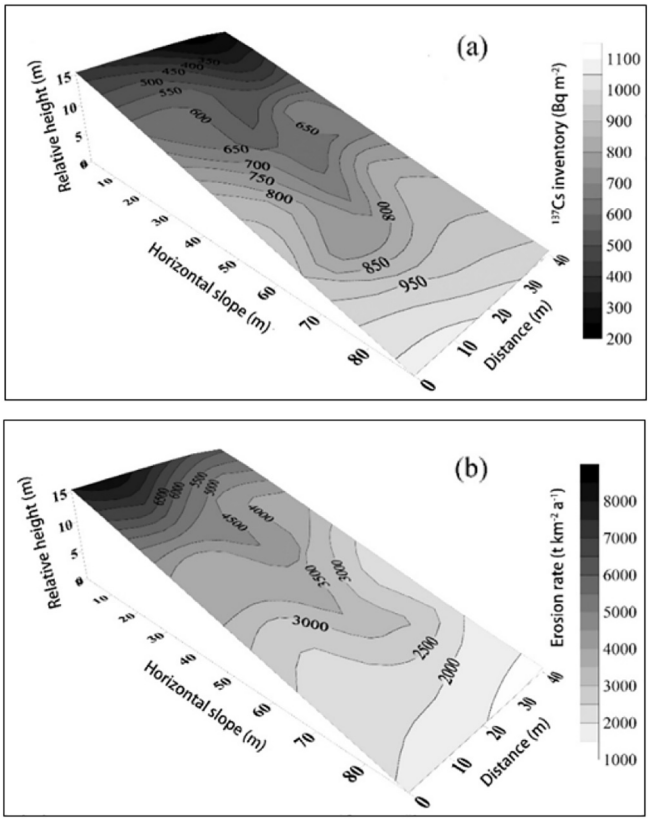

Fig. 2. The distributions of soil ^{137}Cs inventories (a) and erosion rates (b) on slope cultivated land (S7 slope site).

3.3.1. SOC and TN contents

The SOC content was 5.50% higher on the southeast- than the northwest-facing slopes and ranged from 6.58 to 8.32 g kg^{-1} and 6.31 to 7.25 g kg^{-1} on the southeast- and northwest-facing slopes, respectively (Table 3). The SOC content increased down the slopes for both aspects and was highest at the bottom SPs and lowest at the upper SPs. The SOC content was significantly lower by 22.9% in the 0–5 cm layer compared to the 10–20 cm layer on the northwest-facing slopes ($p < 0.01$) but did not differ significantly on the southeast-facing slopes ($p > 0.05$).

The effects of SA and SP on the TN content were similar to those on the SOC content. The TN content was 31.67% higher on the southeast- than the northwest-facing slopes and ranged from 0.47 to 0.64 g kg^{-1} and 0.33 to 0.40 g kg^{-1} on the southeast- and northwest-facing slopes, respectively (Table 3). The TN content was highest at the bottom SPs (0.64 g kg^{-1}) on the southeast-facing slopes and lowest at the upper SPs (0.33 g kg^{-1}) on the northwest-facing slopes. The TN content was

Table 3
Soil physicochemical properties for the slope aspects and positions.

Topographic factors		Chemical properties		Physical properties		
		SOC content (g kg^{-1})	TN content (g kg^{-1})	Sand content (%)	Silt content (%)	Clay content (%)
Northwest-facing slope	Slope position					
	Upper	6.64 ± 1.58^{a}	0.33 ± 0.01^{b}	76.29 ± 0.88^{a}	15.30 ± 0.50^{a}	8.41 ± 0.37^{a}
	Middle	6.31 ± 0.64^{a}	0.39 ± 0.02^{a}	75.57 ± 0.85^{a}	15.65 ± 0.60^{a}	8.78 ± 0.28^{a}
	Lower	6.80 ± 0.82^{a}	0.40 ± 0.01^{a}	76.07 ± 0.46^{a}	15.09 ± 0.28^{a}	8.79 ± 0.23^{a}
	Bottom	7.25 ± 0.51^{a}	0.39 ± 0.00^{a}	75.63 ± 0.34^{a}	15.51 ± 0.08^{a}	8.85 ± 0.26^{a}
	Soil depth					
	0–5 cm	5.96 ± 0.12^{b}	0.36 ± 0.03^{a}	76.41 ± 0.41^{a}	15.12 ± 0.23^{a}	8.46 ± 0.25^{b}
	5–10 cm	6.55 ± 0.96^{ab}	0.38 ± 0.02^{a}	75.74 ± 0.90^{a}	15.47 ± 0.64^{a}	8.75 ± 0.37^{ab}
	10–20 cm	7.73 ± 0.65^{a}	0.39 ± 0.04^{a}	75.52 ± 0.15^{a}	15.57 ± 0.20^{a}	8.91 ± 0.10^{a}
Southeast-facing slope	Slope position					
	Upper	6.58 ± 0.31^{c}	0.47 ± 0.01c	71.61 ± 1.01^{a}	18.31 ± 0.80^{b}	10.08 ± 0.22^{a}
	Middle	6.41 ± 0.39^{c}	0.53 ± 0.01^{b}	70.36 ± 0.02^{ab}	19.37 ± 0.19^{ab}	10.27 ± 0.20^{a}
	Lower	7.26 ± 0.19$_{b}$	0.57 ± 0.02^{a}	69.65 ± 1.35^{b}	19.88 ± 0.86^{ab}	10.47 ± 0.49^{a}
	Bottom	8.32 ± 0.27^{a}	0.64 ± 0.02^{a}	68.97 ± 1.03^{b}	20.36 ± 0.63^{a}	10.67 ± 0.40^{a}
	Soil depth					
	0–5 cm	6.94 ± 1.04^{a}	0.54 ± 0.07^{a}	70.93 ± 1.17^{a}	19.02 ± 1.01^{a}	10.05 ± 0.17^{b}
	5–10 cm	7.07 ± 0.72^{a}	0.55 ± 0.07^{a}	70.26 ± 1.07^{a}	19.32 ± 0.85^{a}	10.41 ± 0.23^{ab}
	10–20 cm	7.42 ± 0.86^{a}	0.56 ± 0.08^{a}	69.25 ± 1.41^{a}	20.09 ± 0.98^{a}	10.66 ± 0.43^{a}

Note: Different letters within a column among slope positions and soil depths indicate significant differences at $p < 0.05$.

lower in the 0–5 than the 10–20 cm soil layer, but the difference was not significant ($p > 0.05$).

3.3.2. Soil particle-size distribution

The sand content ranged from 75.57 to 76.29% and 68.97 to 71.61% on the northwest- and southeast-facing slopes, respectively (Table 3). The sand content was 7.57% higher on the northwest- than southeast-facing slopes, and the clay and silt contents were 21.01 and 16.05% higher on the southeast- than northwest-facing slopes, respectively. In addition, the clay content was significantly lower in the 0–5 than the 10–20 cm layer on both the southeast- and northwest-facing slopes ($p < 0.05$). The sand and silt contents, however, did not clearly differ among the three layers ($p > 0.05$).

3.4. Relationships of ^{137}Cs inventory, SOC content, TN content, and soil texture

Table 4 presents Pearson's correlation coefficients between the ^{137}Cs inventories and soil physicochemical properties for the S1-S6 site in the 0–20 cm soil layer. The ^{137}Cs inventory was positively correlated with the clay and silt contents and negatively correlated with the sand content ($p < 0.05$). The relationships between the ^{137}Cs inventory and SOC and TN contents were described well by linear functions (Fig. 4). The areas with low ^{137}Cs inventories had low SOC and TN contents.

4. Discussion

4.1. Contributions of wind and water erosion to total soil loss

^{137}Cs inventories were used to estimate the degree of total soil erosion. ^{137}Cs fallout is rapidly and irreversibly fixed to soil particles. The reference ^{137}Cs inventory was estimated in an undisturbed, non-

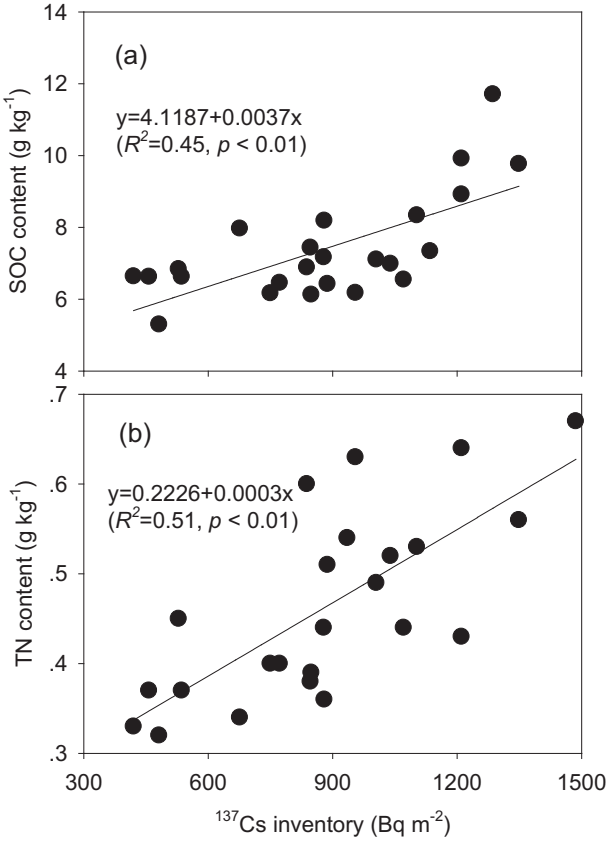

Fig. 4. Relationships between soil ^{137}Cs inventory and SOC (a) and TN (b) contents (slope sites S1–S6).

Table 4
Correlations between ^{137}Cs inventory and soil physicochemical properties.

Parameter	^{137}Cs inventory	SOC content	TN content	Sand content	Silt content	Clay content
^{137}Cs inventory	1	0.472*	0.549**	−0.440*	0.418*	0.451*
SOC content		1	0.470*	−0.435*	0.438*	0.499*
TN content			1	−0.802**	0.815**	0.722**
Sand content				1	−0.993**	−0.959**
Silt content					1	0.920**
Clay content						1

Note: * and ** indicate significance at 0.05 and 0.01 lever, respectively.

eroded and flat forest sites where the vegetation is dominated by *Locust*. Generally, plant canopy determines the size and velocity of raindrops, while soil redistribution and particle selectivity depends on the energy of the raindrops (Wang and Shi, 2015). In our study, the canopy densities (>85%) are higher, and there is less bare soil in the *Locust* stands (55 years) than in the study area. After being intercepted by the canopy, the energy of the raindrops declines when they reach the soil; thus, the soil loss (i.e., ^{137}Cs migration) can be ignored. Although this hypothesis is not exact, we believe that this did not bias the soil redistribution estimations due to the large variations in climate (Van Pelt et al., 2017). The reference ^{137}Cs inventory in our study (1449 Bq m^{-2}) was similar to the result observed by Li et al. (2005), who calculated a ^{137}Cs reference inventory of 1580 Bq m^{-2} from soil samples on the Chinese Losses Plateau.

The present study selected three northwest-facing slopes (S1-S3), three southeast-facing slopes (S4-S6), and a typical northwest-facing slope (S7). The erosion rates on these slopes were 3396 t km^{-2} y^{-1}, 2139 t km^{-2} y^{-1}, and 3731 t km^{-2} y^{-1}, respectively, with an average of 3089 t km^{-2} y^{-1}. By using geographic information systems and the RUSLE, Qin et al. (2019) estimated the average annual soil erosion in the Simianyangou watershed of our study area, which ranged from 3251 to 5927 t km^{-2} y^{-1}. Although this value was higher than our results, we believe that the data obtained in our study are credible considering the simulation errors and effect of topography. In addition, the northwest-facing slopes that we selected faced an open valley, and the dominant wind direction was from the north and northwest, as mentioned in Section 2.1. Thus, the northwest-facing slopes directly faced the winds and suffered from serious wind erosion. By contrast, the southeast-facing slopes were on the leeward side, and wind erosion should be lower on these slopes than for the other aspects (Li et al., 2005). The present study demonstrated that the erosion rates on northwest-facing slopes (S1–S3) were 58.8% higher than those on southeast-facing slopes (S4–S6). By observing and analysing, we can infer that wind erosion could have probably promoted this difference in soil loss between the southeast- and northwest-facing slopes. Based on the ^{137}Cs measurements and the RUSLE model for slope site S7, wind erosion was estimated to approximately 39.7% of total soil loss in the study area on the Chinese Loess Plateau. Interestingly, this value was consistent with the result (>18%) observed by Li et al. (2005) in the wind-water erosion crisscross region in Shenmu City on Chinese Loess Plateau.

4.2. Response of soil physicochemical properties to wind and water erosion

Water erosion involves the detachment and transport of soil materials via raindrop impacts and runoff scouring (Issa et al., 2006; Shi et al., 2012b). The energy of raindrops can impact the redistribution of soil and particle selectivity (Wang and Shi, 2015; Hu et al., 2016). Wind erosion is a dynamic process that coarsens soil texture (Dong and Qian, 2007). Both wind and water erosion preferentially remove finer particles (i.e., small sizes including clay and silt) and lead to high concentrations of soil nutrients and fine particles in soil sediments (Visser and Sterk, 2007; Tuo et al., 2016). The results showed that the northwest-facing slopes experienced higher soil erosion and thus have lower clay and silt contents than the southeast-facing slopes. In addition, wind erosion may have a direct influence on water erosion in regions where both types of erosion occur. Wind erosion can destroy the soil structure and loosen the ground surface material, providing the conditions upon which water erosion can act more easily than without preceding wind erosion (Song et al., 2005). Soil properties also affect the transport of soil materials under the impacts of raindrop detachment and runoff. For example, soil water retention, soil infiltration and hydraulic conductivity can influence the temporal variations in soil erosion (Ouyang et al., 2018). Northwest-facing slopes in our study have coarser particles than the southeast-facing slopes, which probably results in higher soil erosion. As a result, the present study demonstrated that the soil properties were directly linked to soil redistribution. Soil erosion affects soil nutrients not only because of its impact on soil physical properties but also because it induces a net soil loss, and then produces a net soil nutrients loss.

Terrain is a very important factor that affects soil nutrient contents in hilly areas. Generally, the direction of sediment transport is generally controlled by wind direction for wind erosion and by topography for water erosion (Visser et al., 2004). Slope runoff carries fine particles of soil from upper positions to the lower positions (Shi et al., 2012a). Wind erosion has a stronger effect on the selective transport of soil particles in the upper parts of the slope than in the bottom parts of the slope due to the higher terrain, resulting in the exacerbation of the soil particle redistribution in the uphill sections. As a result, the lowest ^{137}Cs inventories and the lowest SOC, TN, clay, and silt contents were obtained at the upper SPs on the northwest-facing slopes, which were attributed to the complex erosion forces by wind and water and their interaction in the same area. In addition, soil water content may be another factor that affects the spatial patterns of SOC and TN contents (Jia et al., 2017). Compared to the southeast-facing slope, the northwest-facing slopes in our findings had lower soil water contents due to the higher winds and more direct sunlight. The higher soil water content on the southeast-facing slope was generally found to promote plant growth and increase litter production, which provides soil C and N sources via decomposition processes (Sigua and Coleman, 2010).

Interestingly, the SOC and TN contents in our study were slightly lower in the topsoil (0–5 cm) than the 5–10 and 10–20 cm layers (Table 3), which is perhaps due to the severe wind erosion that occurred in the winter and spring. The soil samples in our study were collected during the spring in May, and the soils at the surface were subject to wind erosion only after they were ploughted to the 20 cm depth. Thus, fine soil particles would have been removed by wind erosion during the winter and spring, which would decrease the nutrient contents (Pires et al., 2017). Sigua and Coleman (2010) noted that nearly 77% of the variability in the concentration of soil organic carbon was due to the soil clay content. Soil nutrient losses by wind erosion cannot be negligible at a field scale, compared to water erosion (Yan et al., 2005; Visser and Sterk, 2007). For example, Buerkert and Hiernaux (1998) reported that nearly 15 kg N and 2 kg P ha^{-1} y^{-1} were lost from traditionally cultivated fields due to wind erosion. Yan et al. (2005) estimated that approximately 75 Tg C y^{-1} of organic carbon was lost from the surface horizon in eroded regions in China because of wind erosion.

4.3. Implications and future work

The selected sloped croplands in our study had been converted from forest prior to the 1950s due to the long history of crop production and expanding human population (Jia et al., 2017). Our results showed that the mean ^{137}Cs inventories on the northwest-facing slopes (749 Bq m^{-2}) and the southeast-facing slopes (1015 Bq m^{-2}) were lower than that at the reference site, demonstrating that the landscape over the last 55 years has experienced substantial net erosion. The physical degradation of soils through erosion is associated with chemical degradation. Wind and water erosion control the movement of water and material on hillslopes and substantially contribute to overall soil degradation (Visser and Sterk, 2007; Belnap et al., 2011). Middleton and Thomas (1997) noted that wind and water erosion could account for >85% of the soil degradation in dryland areas. This degradation process does not only lead to losses of soil particles but also leads to reductions in plant nutrients and water storage capability, resulting in the severe decline of crop yields and environmental quality (Pansak et al., 2008).

Soil erosion intensity mainly depends on topographical factors, the size and velocity of raindrops, and the interception of raindrops or winds by the canopy and floor cover, which would reduce the erosive power (Li et al., 2017b). The water erosion rate (2216 t km^{-2} a^{-1}) in our study was higher than the wind erosion rate (1460 t km^{-2} a^{-1}). Although the control of soil loss should fully consider the different impacts

of water and wind erosion, our results indicated that taking some measures (such as check dams and terraces) to reduce water erosion can maximize the reduction in total soil erosion. In addition, the different tree species and vegetation cover had different soil erosion control and soil C and N sequestration benefits (Jia et al., 2017). Feng et al. (2017) noted that planting *Hippophae rhamnoides* was an optimal choice for soil erosion control and soil carbon loss mitigation in the loess hilly-gully region. Alliaume et al. (2014) reported that stubble mulch and no-till management could be a feasible alternative to reduce the susceptibility of erosion by wind and water. Consequently, topographic factors could regulate erosion control and nutrient accumulation; thus, we must consider the corresponding influencing factors to regulate ecosystem services. These measures include building bench terraces to fully utilize soil and water resources and implementing no-till management on northwest-facing slopes to control total soil erosion.

5. Conclusions

Wind and water erosion alternately occur on the Loess Plateau and are affected by wind direction and topography, respectively. Based on the ^{137}Cs inventories among different slope aspects and positions, this study indicated that total soil erosion was much more intense at the upper positions than at the other positions, and total soil erosion was higher on northwest-facing slopes than on southeast-facing slopes. Soil properties were linked to soil erosion at different topographic positions. Soil erosion affects soil nutrients not only because of its impact on soil physical properties but also because it induces a net soil loss. The lowest SOC and TN contents were obtained at the upper positions on the northwest-facing slopes due to severe wind and water erosion. The results indicated that complex erosion by wind and water accelerated the degradation of the soil quality.

Based on the differences in erosion amount of the typical selected slope land that were identified using the RUSLE model and ^{137}Cs measurements, we found that the water erosion rate (2216 t km^{-2} a^{-1}) was higher than the wind erosion rate (1460 t km^{-2} a^{-1}). Wind erosion accounted for 39.7% of the total erosion, and water erosion accounted for 60.3%. Control water erosion could effectively reduce soil loss as compared to the control wind erosion. The results will provide a valuable reference for researchers to develop soil strategies to reduce soil erosion according to the type of erosion that dominates the year when it occurs in a hilly agricultural area.

Acknowledgments

This research was financially supported by the National Natural Science Foundation of China (no. 41771318), and by the National Key Research and Development Program of China (no. 2016YFC0501602). We thank the four anonymous reviewers for their constructive comments which improve the quality of this manuscript.

References

Afshar, F.A., Ayoubi, S., Jalalian, A., 2010. Soil redistribution rate and its relationship with soil organic carbon and total nitrogen using ^{137}Cs technique in a cultivated complex hillslope in western Iran. J. Environ. Radioact. 101, 606–614.

Alliaume, F., Rossing, W.A.H., Tittonell, P., Jorge, G., Dogliotti, S., 2014. Reduced tillage and cover crops improve water capture and reduce erosion of fine textured soils in raised bed tomato systems. Agric. Ecosyst. Environ. 183, 127–137.

An, J., Zheng, F.L., Wang, B., 2014. Using ^{137}Cs technique to investigate the spatial distribution of erosion and deposition regimes for a small catchment in the black soil region, Northeast China. Catena 123, 243–251.

Belnap, J., Munson, S.M., Field, J.P., 2011. Aeolian and fluvial processes in dryland regions: the need for integrated studies. Ecohydrology 4, 615–622.

Bowker, M.A., Belnap, J., Chaudhary, V.B., Johnson, N.C., 2008. Revisiting classic water erosion models in drylands: the strong impact of biological soil crusts. Soil Biol. Biochem. 40, 2309–2316.

Bremner, J.M., Mulvaney, C.S., 1982. Nitrogen-total. In 'Methods of soil analysis. Part 2'. In: Page, A.L., Miller, R.H., Keeney, D.R. (Eds.), Agronomy Monograph 9. ASA and SSSA, Madison, WI, pp. 595–614.

Breshears, D.D., Whicker, J.J., Johansen, M.P., Pinder, J.E., 2003. Wind and water erosion and transport in semi-arid shrubland, grassland and forest ecosystems: quantifying dominance of horizontal wind-driven transport. Earth Surf. Process. Landf. 28, 1189–1209.

Buerkert, A., Hiernaux, P., 1998. Nutrients in West African Sudano–Sahelian zone: losses transfers and role of external inputs. J. Plant Nutr. Soil Sci. 161, 365–383.

Conforti, M., Buttafuoco, G., 2017. Assessing space-time variations of denudation processes and related soil loss from 1955 to 2016 in southern Italy (Calabria region). Environ. Earth Sci. 76, 457.

Conforti, M., Buttafuoco, G., Rago, V., Aucelli, P.P.C., Robustelli, G., Scarciglia, F., 2016. Soil loss assessment in the Turbolo catchment (Calabria, Italy). J. Maps 12, 815–825.

Dong, Z.B., Qian, G.Q., 2007. Characterizing the height profile of the flux of wind-eroded sediment. Environ. Geol. 51, 835–845.

Du, H., Wang, T., Xue, X., 2017. Potential wind erosion rate response to climate and land-use changes in the watershed of the Ningxia-Inner Mongolia reach of the Yellow River, China, 1986–2013. Earth Surf. Process. Landf. 42, 1923–1937.

Fang, H.Y., Li, Q.Y., Sun, L.Y., Cai, Q.G., 2012. Using ^{137}Cs to study spatial patterns of soil erosion and soil organic carbon (SOC) in an agricultural catchment of the typical black soil region, Northeast China. J. Environ. Radioact. 112, 125–132.

Feng, Q., Zhao, W.W., Fu, B.J., Ding, J.Y., Wang, S., 2017. Ecosystem service trade-offs and their influencing factors: a case study in the Loess Plateau of China. Sci. Total Environ. 607–608, 1250–1263.

Galy, V., Peucker-Ehrenbrink, B., Eglinton, T., 2015. Global carbon export from the terrestrial biosphere controlled by erosion. Nature 521, 204–207.

Gao, G.Y., Fu, B.J., Lu, Y.H., Liu, Y., Wang, S., Zhou, J., 2012. Coupling the modified SCS-CN and RUSLE models to simulate hydrological effects of restoring vegetation in the Loess Plateau of China. Hydrol. Earth Syst. Sci. 16, 2347–2364.

Gao, L.Q., Bowker, M.A., Xu, M.X., Sun, H., Tuo, D.F., Zhao, Y.G., 2017. Biological soil crusts decrease erodibility by modifying inherent soil properties on the Loess Plateau, China. Soil Biol. Biochem. 105, 49–58.

Hu, W., Zheng, F.L., Bian, F., 2016. The directional components of splash erosion at different raindrop kinetic energy in the Chinese mollisol region. Soil Sci. Soc. Am. J. 80, 1329–1340.

Issa, O.M., Le Bissonnais, Y., Planchon, O., Favis-Mortlock, D., Silvera, N., Wainwright, J., 2006. Soil detachment and transport on field-and laboratory-scale interrill areas: erosion processes and the size-selectivity of eroded sediment. Earth Surf. Process. Landf. 31, 929–939.

Jia, X., Yang, Y., Zhang, C., Shao, M., Huang, L., 2017. A state-space analysis of soil organic carbon in China's Loess Plateau. Land Degrad. Dev. 28, 983–993.

Khaleghpanah, N., Shorafa, M., Asadi, H., Gorji, M., Davari, M., 2016. Modeling soil loss at plot scale with EUROSEM and RUSLE2 at stony soils of Khamesan watershed, Iran. Catena 147, 773–788.

Li, M., Li, Z.B., Liu, P.L., Yao, W.Y., 2005. Using Cesium-137 technique to study the characteristics of different aspect of soil erosion in the wind-water erosion crisscross region on Loess Plateau of China. Appl. Radiat. Isot. 62, 109–113.

Li, P.F., Mu, X.M., Holden, J., Wu, Y.P., Irvine, B., Wang, F., Gao, P., Zhao, G.J., Sun, W.Y., 2017a. Comparison of soil erosion models used to study the Chinese Loess Plateau. Earth-Sci. Rev. 170, 17–30.

Li, Z.W., Liu, C., Dong, Y.T., Chang, X.F., Nie, X.D., Liu, L., Xiao, H.B., Lu, Y.M., Zeng, G.M., 2017b. Response of soil organic carbon and nitrogen stocks to soil erosion and land use types in the Loess hilly–gully region of China. Soil Tillage Res. 166, 1–9.

Martínez-Graña, A.M., Goy, J.L., Zazo, C., 2014. Water and wind erosion risk in natural parks. A case study in "Las Batuecas-Sierra de Francia" and "Quilamas" protected parks (Central System, Spain). Int. J. Environ. Res. 8, 61–68.

Martínez-Graña, A.M., Goy, J.L., Zazo, C., 2015. Cartographic procedure for the analysis of eolian erosion hazard in Natural Parks (Central System, Spain). Land Degrad. Dev. 26, 110–117.

Middleton, N., Thomas, D., 1997. World Atlas of Desertification. 2nd edn. Arnold, London, UK.

Nearing, M.A., 1997. A single continuous function for slope steepness influence on soil loss. Soil Sci. Soc. Am. J. 61, 917–919.

Nelson, D.W., Sommer, L.E., 1982. Total carbon, organic carbon, and organic matter. In: Page, A.L., Miller, R.H., Keeney, D.R. (Eds.), Methods of Soil Analysis. American Society of Agronomy and Soil Science Society of American, Madison, pp. 1–129.

Nie, X.J., Zhao, T.Q., Qiao, X.N., 2013. Impacts of soil erosion on organic carbon and nutrient dynamics in an alpine grassland soil. Soil Sci. Plant Nutr. 59, 660–668.

Ouyang, W., Wu, Y.Y., Hao, Z.C., Zhang, Q., Bu, Q.W., Gao, X., 2018. Combined impacts of land use and soil property changes on soil erosion in a mollisol area under long-term agricultural development. Sci. Total Environ. 613-614, 798–809.

Pansak, W., Hilger, T.H., Dercon, G., Kongkaew, T., Cadisch, G., 2008. Changes in the relationship between soil erosion and N loss pathways after establishing soil conservation systems in uplands of Northeast Thailand. Agric. Ecosyst. Environ. 128, 167–176.

Parsons, A.J., Foster, I.D.L., 2011. What can we learn about soil erosion from the use of ^{137}Cs? Earth-Sci. Rev. 108, 101–113.

Pires, C.V., Schaefer, C.E.R.G., Hashigushi, A.K., Thomazini, A., Filho, E.I.F., Mendonça, E.S., 2017. Soil organic carbon and nitrogen pools drive soil C-CO2 emissions from selected soils in Maritime Antarctica. Sci. Total Environ. 596-597, 124–135.

Qin, W., Zhu, Q.K., Zhang, Y., 2009. Soil erosion assessment of small watershed in Loess Plateau based on GIS and RUSLE. Trans. CSAE 25, 157–163 (in Chinese with English abstract).

Rendard, K.G., Foster, G.R., Weesies, G.A., McCool, D.K., Yoder, D.C., 1997. Predicting Soil Erosion by Water: A Guide to Conservation Planning with the Revised Universal

Soil Loss Equation (RUSLE), Agricultural Handbook, No. 703. US Department of Agriculture, Washington, D.C.
Schmidt, J., Werner, M.V., Schindewolf, M., 2017. Wind effects on soil erosion by water — a sensitivity analysis using model simulations on catchment scale. Catena 148, 168–175.
Sharply, N., Williams, J.R., 1990. EPIC-Erosion Productivity Impact Calculator: 1. Model Documentation. USDA Tech. Bull. No. 1768.
Shi, Z.H., Fang, N.F., Wu, F.Z., Wang, L., Yue, B.J., Wu, G.L., 2012a. Soil erosion processes and sediment sorting associated with transport mechanisms on steep slopes. J. Hydrol. 454, 123–130.
Shi, Z.H., Yue, B.J., Wang, L., Fang, N.F., 2012b. Effects of mulch cover rate on interrill erosion processes and the size selectivity of eroded sediment on steep slopes. Soil Sci. Soc. Am. J. 77, 257–267.
Sigua, G.C., Coleman, S.W., 2010. Spatial distribution of soil carbon in pastures with cow-calf operation: effects of slope aspect and slope position. J. Soils Sediments 10, 240–247.
Song, Y., Yan, P., Liu, L.Y., 2005. A review of the research on complex erosion by wind and water. J. Geogr. Sci. 16, 231–241.
Tiwari, A., Risse, L., Nearing, M., 2000. Evaluation of WEPP and its comparison with USLE and RUSLE. Trans. ASAE 43, 1129–1135.
Tuo, D.F., Xu, M.X., Zhao, Y.G., Gao, L.Q., 2015. Interactions between wind and water erosion change sediment yield and particle distribution under simulated conditions. J. Arid. Land 7, 590–598.
Tuo, D.F., Xu, M.X., Gao, L.Q., Zhang, S., Liu, S.H., 2016. Changed surface roughness by wind erosion accelerates water erosion. J. Soils Sediments 16, 105–114.
Van Pelt, R.S., Hushmurodov, S.X., Baumhardt, R.L., Chappell, A., Nearing, M.A., Polyakov, V.O., Strack, J.E., 2017. The reduction of partitioned wind and water erosion by conservation agriculture. Catena 148, 160–167.
Visser, S.M., Sterk, G., 2007. Nutrient dynamics–wind and water erosion at the village scale in the Sahel. Land Degrad. Dev. 18, 578–588.
Visser, S.M., Sterk, G., Ribolzi, O., 2004. Techniques for simultaneous quantification of wind and water erosion in semi-arid regions. J. Arid Environ. 59, 699–717.
Walling, D.E., He, Q., 1999. Improved models for estimating soil erosion rates from caesium-137 measurements. J. Environ. Qual. 28, 611–622.
Wang, L., Shi, Z.H., 2015. Size selectivity of eroded sediment associated with soil texture on steep slopes. Soil Sci. Soc. Am. J. 79, 917–929.
Wang, X., Zhao, X.L., Zhang, Z.X., Yi, L., Zuo, L.J., Wen, Q.K., Liu, F., Xu, J.Y., Hu, S.G., Liu, B., 2016. Assessment of soil erosion change and its relationship with land use/cover change in China from the end of the 1980s to 2010. Catena 137, 256–268.
Xue, Z.J., Qin, Z.D., Cheng, F.Q., Ding, G.W., Li, H.J., 2017. Quantitative assessment of aeolian desertification dynamics-a case study in north Shanxi of China (1975 to 2015). Sci. Rep. 7, 10460.
Yan, H., Wang, S.Q., Wang, C.Y., Zhang, G.P., Patel, N.C., 2005. Losses of soil organic carbon under wind erosion in China. Glob. Chang. Biol. 11, 828–840.
Zhang, Y.G., Nearing, M.A., Liu, B.Y., Van Pelt, R.S., Stone, J.J., Wei, H., Scott, R.L., 2011. Comparative rates of wind versus water erosion from a small semiarid watershed in southern Arizona, USA. Aeolian Res. 3, 197–204.
Zhang, J.Q., Yang, M.Y., Deng, X.X., Liu, Z., Zhang, F.B., Zhou, W.Y., 2018. Beryllium-7 measurements of wind erosion on sloping fields in the wind-water erosion crisscross region on the Chinese Loess Plateau. Sci. Total Environ. 615, 240–252.